Green Chemical Engineering xxx (xxxx) xxx

Contents lists available at ScienceDirect

Green Chemical Engineering

journal homepage: www.keaipublishing.com/en/journals/green-chemical-engineering

Article

Tuning cationic structures in ionic liquids for enhanced sulfur dioxide absorption-desorption and mass transfer efficiency

Wei Hui[a,b], Xin Wang[a], Xiao-Ya Wang[b], Fei-Feng Mao[b], Tiao Zhang[a], Yan Zhou[b,*], Jia-Yin Zhang[b,**], Duan-Jian Tao[b,***]

[a] School of Life Science, Key Laboratory of Jiangxi Province for Functional Biology and Pollution Control in Red Soil Regions, Jinggangshan University, Ji'an, 343009, China

[b] School of Chemical Engineering, Key Laboratory of Functional Small Molecules for Ministry of Education, Jiangxi Normal University, Nanchang, 330022, China

HIGHLIGHTS

- $DiEtSO_4$-based ILs with different viscosities (3–285 cP) were designed.
- A quantitative model was proposed to correlate ILs viscosity with SO_2 mass transfer.
- DFT, COSMOtherm, IGM, thermodynamic and kinetic analyses were performed.
- [MIM][$DiEtSO_4$] exhibited high SO_2 absorption performance and reusability.

GRAPHICAL ABSTRACT

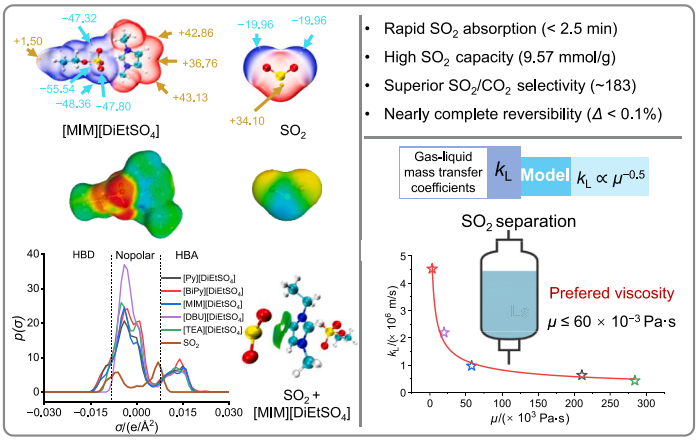

ARTICLE INFO

Keywords:
Ionic liquids
Sulfur dioxide
Absorption
Mass transfer kinetics
Viscosity

ABSTRACT

The mass transfer and diffusion limitations of ionic liquids (ILs) have hindered their application in SO_2 separation. In this work, five diethyl sulfate ($DiEtSO_4$) based ionic liquids ($DiEtSO_4$-based ILs) with different viscosities (μ, 3–285 cP) were synthesized by tuning the cationic structures. The SO_2 absorption capacities and kinetics of $DiEtSO_4$-based ILs were evaluated at 298–313 K. Meanwhile, liquid-side volumetric mass transfer coefficients (k_La) and liquid-side mass transfer coefficients (k_L) were determined using the pressure drop method to assess SO_2 mass transfer in $DiEtSO_4$-based ILs quantitatively. The results indicated a physical absorption mechanism for SO_2, consistent with Henry's law (ΔH < ~21 kJ/mol). Specifically, both 1-methylimidazole diethyl sulfate ([MIM][$DiEtSO_4$]) and 1,8-diazabicyclo[5.4.0]undec-7-ene diethyl sulfate ([DBU][$DiEtSO_4$]

Peer review under the responsibility of Editorial Board of Green Chemical Engineering.

* Corresponding author.
** Corresponding author.
*** Corresponding author.
E-mail addresses: anitachow@jxnu.edu.cn (Y. Zhou), jy_zhang@jxnu.edu.cn (J.-Y. Zhang), djtao@jxnu.edu.cn (D.-J. Tao).

https://doi.org/10.1016/j.gce.2025.12.005
Received 28 September 2025; Received in revised form 8 December 2025; Accepted 25 December 2025
Available online xxxx

Please cite this article as: W. Hui et al., Tuning cationic structures in ionic liquids for enhanced sulfur dioxide absorption-desorption and mass transfer efficiency, Green Chemical Engineering, https://doi.org/10.1016/j.gce.2025.12.005

demonstrated high capacities (~9.6 mmol/g), rapid kinetics (equilibrium within < 2.5 min), and excellent cyclic stability with minimal capacity loss (~0.1%). Moreover, density functional theory (DFT), conductor-like screening model for real solvent thermodynamics (COSMOtherm), and independent gradient model (IGM) analyses confirmed that van der Waals and weak electrostatic interactions predominate over chemical bonding in the absorption process. Mass transfer analysis confirmed an inverse relationship between μ and k_L ($k_L \propto \mu^{-0.5}$) in $DiEtSO_4$-based ILs, which is consistent with Danckwerts' theory. Based on its superior overall performance in SO_2 absorption capacity, mass transfer rate, and cyclic stability, [MIM][$DiEtSO_4$] emerged as the most promising candidate for SO_2 separation and recovery.

1. Introduction

Sulfur dioxide (SO_2) is recognized as a major air pollutant, primarily released from the combustion of fossil fuels such as coal and oil. It is a serious threat to human health and environmental safety through the formation of acid rain or $PM_{2.5}$ particles [1–3]. At the same time, SO_2 also serves as a valuable sulfur-containing feedstock for the synthesis of fine chemicals, including pesticides, food additives, and pharmaceutical intermediates [4–6]. The annual emissions exceeding 73 million tons of SO_2 from global industrial activities present a pressing environmental challenge and a substantial opportunity for recovering sulfur resources [7]. Thus, the development of efficient and sustainable technologies for SO_2 separation and recovery has attracted significant attention from environmental and chemical engineering perspectives.

Currently, various absorption-based separation techniques are widely used in industrial applications [8–11]. Ionic liquids (ILs) offer adjustable polarity, excellent thermal stability, specific intermolecular interactions, and excellent thermal stability owing to their structurally designable molecular architectures and negligible vapor pressures [12–14]. Moreover, deep eutectic solvents (DESs), which share similar properties with ILs, have likewise attracted extensive attention and application in gas separation processes [15]. These properties render them widely recognized as green alternatives to conventional absorbents and as promising SO_2 absorbents. Nevertheless, ILs and DESs generally suffer from capacity loss upon cyclic SO_2 absorption-desorption operation. This limitation is mainly attributed to the predominance of chemical interactions during SO_2 uptake, which inevitably leads to residual absorption after regeneration. For example, Wang et al. [16] reported that tributylethylphosphonium bis(trifluoromethylsulfonyl)imide (P_{4442}][TFSI]) achieved an SO_2 uptake of 4.27 mol/mol at 293 K and 1 bar. However, it suffered from significant drawbacks, including an 11.71% capacity loss after regeneration and slow kinetics (~13 min to reach saturation) due to high mass transfer resistance. Similarly, Wu et al. [17] demonstrated that L-carnitine + ethylene glycol (L-car + EG, 1:3) achieved an SO_2 uptake capacity of 5.78 mmol/g at 313 K and 1 bar, yet suffered from 13.51% capacity decay upon regeneration, with equilibrium times > 60 min. Collectively, these findings highlight that both the slow absorption rate and the capacity loss of ILs remain critical bottlenecks limiting their practical deployment in SO_2 separation and recovery.

Furthermore, the structural diversity of ILs gives rise to substantial variation in physical properties such as density and viscosity, which in turn affect their SO_2 separation performance [18,19]. It is important that the absorption capacity alone is insufficient to evaluate the application value of ILs in gas separation. The mass transfer efficiency also plays a key role in controlling absorption kinetics and energy consumption [20]. In fact, mass transfer is closely related to the physical properties of ILs in gas-liquid systems, with viscosity (μ) identified as a dominant factor. It is well known that elevated μ hinders the diffusion of SO_2 molecules within IL phase, increases mass transfer resistance, and diminishes interfacial renewal rates, thus limiting the efficiency of separation [21,22]. Therefore, studying the relationship between the structures of anions and cations on μ and corresponding mass transfer behavior is essential for the rational design of high-performance IL-based systems for SO_2 separation.

So far, some researchers have used experimental methods such as the pressure drop method to evaluate the mass transfer coefficients of common absorbents such as water [23,24], ILs [25–27], and organic solvents [28,29] in different gas separation systems and have reported the corresponding liquid side mass transfer coefficients (k_L). For example, Zhang et al. [25] studied the CO_2 absorption performance of imidazolium-based ILs (*e.g.*, 1-butyl-3-methylimidazolium nitrate, [bmim][NO_3]) and determined that liquid-side volumetric mass transfer coefficients (k_La) values were within the range of 0.64–1.52 × 10^5 m/s at 303 K. It is worth noting that the study also found that the addition of monoethanolamine (MEA) aqueous solution into the imidazolium-based ILs system exerted an inhibitory effect on CO_2 absorption efficiency. Similarly, Zarca et al. [27] measured k_La values of CO in 1-hexyl-3-methylimidazolium chloride ([hmim][Cl]), observing a temperature-dependent increase from 3.4 × 10^{-7} m/s to 10.9 × 10^{-7} m/s at 293–313 K. In contrast, studies on mass transfer behavior (k_La and k_L) of SO_2 in IL-based systems remain relatively limited. Meanwhile, it is worth noting that the SO_2 absorption mechanism in most pure ILs involves a synergistic interplay between physical dissolution and chemical interaction, which improves the absorption capacity of ILs under low SO_2 partial pressure. However, determination of k_La and k_L is typically valid only under conditions dominated by physical absorption, as described by the classical Whitman two-film theory [30,31]. The molecular diffusion of the gaseous solute within the liquid phase constitutes the rate-controlling step of the mass transfer process [32]. In addition, the relationship between the ionic structure, μ, and mass transfer behavior (k_La and k_L) is essential for optimizing separation performance of IL in engineering applications. Therefore, it is meaningful to develop ILs with minimal chemical interaction with SO_2 and to explore the effect of ionic structures of ILs on μ and mass transfer.

Herein, a series of $DiEtSO_4$ (diethyl sulfate)-based ILs was synthesized by tuning the cation structures to regulate μ across a broad range (~3–285 cP). These $DiEtSO_4$-based ILs were subsequently evaluated for SO_2 absorption *via* isothermal and isobaric experiments to elucidate the impacts of ionic structures and μ on absorption capacity and kinetics. In addition, the adsorption behavior of $DiEtSO_4$-based ILs for SO_2 has been analyzed by thermodynamic and spectroscopic analysis. Furthermore, k_La and k_L were determined using the pressure drop method, and the Danckwerts model was applied to correlate μ and k_L. Besides, the recyclability and stability of $DiEtSO_4$-based ILs were assessed over ten consecutive SO_2 absorption–desorption tests, which revealed that $DiEtSO_4$-based ILs are viable candidates for SO_2 separation. Overall, this work aims to uncover the mass transfer characteristics of promising IL-based SO_2 separation systems for the rational design of high-performance absorbents.

2. Experimental

2.1. Materials

Diethyl sulfate ($DiEtSO_4$, ≥ 99%) and 4,4-bipyridine (BiPy, ≥ 98%) were obtained from Shanghai Macklin Biochemical Technology Co. Ltd. 1,8-Diazabicyclo[5.4.0]undec-7-ene (DBU, ≥ 99%), triethylamine (TEA, 99%), and pyridine (Py, 99%) were obtained from Shanghai Adamas Reagent Co. Ltd. 1-Methylimidazole (MIM, ≥ 98%) was purchased from Shanghai Aladdin Biochemical technology Co. Ltd. Gases such as SO_2 and N_2 (≥ 99.99%) were supplied by Jiangxi Huate Special Gas Co. Ltd.

In addition, the other reagents were obtained commercially and used directly.

2.2. Synthesis

$DiEtSO_4$-based ILs were synthesized by tuning the cation type in equimolar amounts. The preparation schematics and their structures are given in Fig. 1. In the synthesis of the [MIM][$DiEtSO_4$]: Firstly, 50 mL of ethanol was added into a 100 mL round-bottom flask, followed by the addition of MIM (2 mmol). Subsequently, $DiEtSO_4$ (2 mmol) was added dropwise under vigorous stirring, and the mixture was allowed to react in an ice-water bath for 12 h. Then, the solvent was removed by rotary evaporator at 323 K to obtain the crude ILs. Next, the crude ILs were washed with ethyl acetate (5 × 10 mL) and dried under vacuum at 353 K overnight to obtain pure 1-methylimidazole diethyl sulfate ([MIM][$DiEtSO_4$]). Finally, the other four ILs were prepared using similar synthesis strategies. Furthermore, the structures of $DiEtSO_4$-based ILs were confirmed by ^1H nuclear magnetic resonance (NMR) and ^{13}C NMR on Bruker Avance III HD 400 MHz (Figs. S1-S10). The results of Karl-Fischer titration showed that the water contents of the $DiEtSO_4$-based ILs were lower than 0.05%. The physical properties, such as densities and viscosities of $DiEtSO_4$-based ILs, were determined using an Anton Paar DMA 4500 automatic densitometer and a Brookfield DV II + Pro cone-plate viscometer, respectively.

2.3. SO_2 absorption

The SO_2 absorption experiments were conducted using a custom-built dual-chamber volumetric apparatus (Fig. S11), with detailed structural and operational parameters provided in Supporting Information. The SO_2 absorption capacity of the $DiEtSO_4$-based ILs was determined by subtracting the residual gas content in the equilibrium cell from the initial gas content in the gas reservoir. For the cyclic SO_2 absorption-desorption tests, the following procedure was adopted. After the completion of each SO_2 absorption, the equilibrium cell was depressurized to 0.01 bar, and the SO_2-saturated $DiEtSO_4$-based ILs were heated at 343 K for 2 h to regenerate $DiEtSO_4$-based ILs. The regenerated ILs were then reused for SO_2 absorption in the subsequent run.

2.4. Computational details

In this work, the initial geometries of all molecules were optimized using Gaussian 16. The optimization was performed at the B3LYP/6-311 + G (2d,p) level of theory, with the inclusion of D3(BJ) dispersion correction to account for deviations in the description of weak interactions. To obtain more accurate energy data, single-point energy calculations were subsequently conducted at the def2-TZVP basis set level based on the optimized geometries, and corresponding COSMO files were also generated to provide solvation-related parameters. Electrostatic potential (ESP) analysis and Independent Gradient Model based on Hirshfeld partitioning (IGMH) analysis were carried out using the Multiwfn 3.8 (dev) program [33,34]. Visualization of the resulting data was carried out using visual molecular dynamics (VMD), wherein high-resolution grids were employed to construct color-filled isosurfaces that qualitatively illustrate the spatial distribution of weak interactions between $DiEtSO_4$-based ILs and the SO_2 system. Additionally, the σ-profile and σ-potential of the system were computed using COSMO-therm 2021.

3. Results and discussions

3.1. Physical properties and SO_2 absorption performances

The densities and viscosities of IL absorbents play a key role in the gas absorption process, as they directly affect the efficiency/resistance of gas-liquid mass transfer and the fluid dynamic behavior [25]. The physicochemical properties and SO_2 capture performance of $DiEtSO_4$-based ILs were investigated over 293–353 K, with the corresponding data presented in Fig. 2. The results reveal that temperature profoundly affects both the fluidic characteristics and absorption capacities of these ILs. Fig. 2a–b presents the determined densities and viscosities of $DiEtSO_4$-based ILs at 293–353 K, with associated physical parameters summarized in Table 1. The data were fitted using the empirical models described by Eqs. (S2)-(S3), and the calculated parameters are listed in Table S1. As expected, density and viscosity decrease monotonically with increasing temperature, which is consistent with the typical behavior of liquids wherein elevated thermal energy disrupts intermolecular interactions, thereby reducing these properties. Moreover, it can be found that the slope of the density profiles varied among the ILs, suggesting that specific ionic interactions and cationic structures modulate the thermal response (Fig. 2a). For example, 4,4-bipyridine diethyl sulfate ([BiPy][$DiEtSO_4$]) has a higher density with a lower slope (-6.79×10^{-4}), which may be due to the stronger intermolecular forces caused by the bulkier $[BiPy]^+$ cation. In contrast, triethylamine diethyl sulfate ([TEA][$DiEtSO_4$]) shows a lower density and the highest slope (-9.57×10^{-4}) due to its flexible alkyl chain, which means weaker molecular packing and potentially greater free volume of ILs at higher temperatures. Meanwhile, viscosity trends further reinforce the structure-property relationships, with viscosity decreasing with increasing temperature, which is beneficial for enhancing gas transport kinetics within the ILs. Among the ILs studied, [TEA][$DiEtSO_4$] exhibited the lowest viscosities, whereas [BiPy][$DiEtSO_4$] consistently showed the highest viscosity. These trends may be attributed to the larger steric hindrance and stronger van der Waals interaction of the $[BiPy]^+$ cation compared to the smaller cations in the other $DiEtSO_4$-based ILs.

The impact of molecular structure on SO_2 uptake and viscosity change is crucial for evaluating separation performance. The adsorption isotherms of $DiEtSO_4$-based ILs for SO_2 were tested at 298 K and 1 bar (Fig. 2c and Table 1). It was found that the cationic structures controlled SO_2 capacities of $DiEtSO_4$-based ILs, and their isotherms showed almost linear profiles, which means that SO_2 uptake occurs *via* physical dissolution. Specifically, [MIM][$DiEtSO_4$] and 1,8-diazabicyclo[5.4.0]undec-7-ene diethyl sulfate ([DBU][$DiEtSO_4$]) exhibited the highest SO_2 absorption capacities (~9.6 mmol/g), which may be related to the stronger π-π interaction ability of the $[MIM]^+$ and $[DBU]^+$ cations [35]. In contrast, [TEA][$DiEtSO_4$] and [Py][$DiEtSO_4$] showed lower SO_2 capacities (3.22 mmol/g and 5.61 mmol/g, respectively). In addition, viscosity changes of $DiEtSO_4$-based ILs are presented before and after SO_2 absorption (Fig. 2d). The results indicate that the viscosities of $DiEtSO_4$-based ILs underwent varying degrees of viscosity increase after SO_2 absorption, except for [MIM][$DiEtSO_4$]. It was inferred that the slight decrease in viscosity of [MIM][$DiEtSO_4$] after SO_2 absorption arises

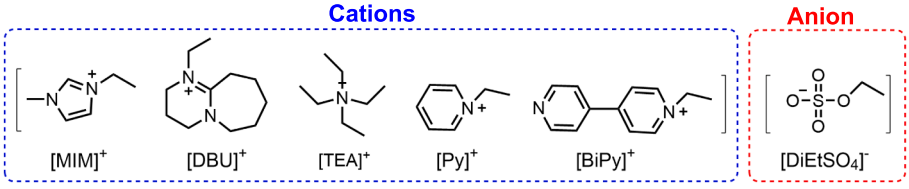

Fig. 1. The cationic and anionic structures of $DiEtSO_4$-based ILs in this work.

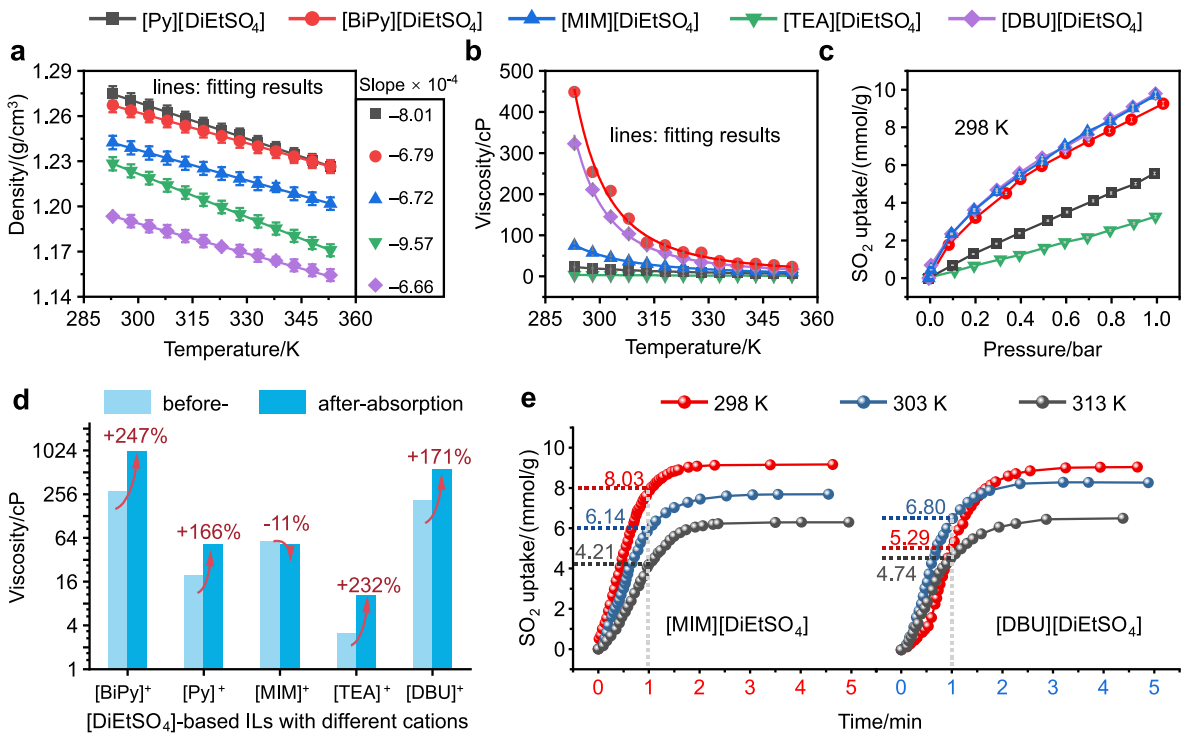

Fig. 2. (a) Densities and (b) viscosities of $DiEtSO_4$-based ILs at 293–353 K; (c) SO_2 absorption isotherms of $DiEtSO_4$-based ILs at 298 K and 1 bar; (d) viscosity changes before and after SO_2 absorption of $DiEtSO_4$-based ILs at 298 K and 1 bar; (e) SO_2 absorption kinetics of [MIM][$DiEtSO_4$] and [DBU][$DiEtSO_4$] at 298–313 K and 1 bar.

from the shielding effect of ionic interactions by SO_2, which weakens the electrostatic or Coulombic interactions between cations and anions in ILs [36,37]. Notably, $DiEtSO_4$-based ILs with $[BiPy]^+$ cation show a viscosity rise, surging 247% from 284.92 cP to 988.44 cP, which was much higher than other heterocyclic cations such as $[DBU]^+$ cation (+171%, from 210.93 cP to 572.31 cP) and $[Py]^+$ cation (+166%, from 19.60 to 52.37 cP). These findings indicate that [MIM][$DiEtSO_4$] achieved a more favorable balance between viscosity and SO_2 absorption capacity. Its viscosity remains relatively stable, even decreasing slightly from 57.96 cP to 51.71 cP (a reduction of 11%), while still maintaining a satisfactory SO_2 capacity (9.57 mmol/g). Furthermore, the surface tensions of [MIM][$DiEtSO_4$] and [DBU][$DiEtSO_4$] were measured at 298–333 K (Fig. S12). The results reveal that above both ILs exhibit a temperature-dependent decrease similar to the trends observed for their density and viscosity, yet the magnitude of this decrease is rather small. In addition, [DBU][$DiEtSO_4$] shows a lower surface tension than [MIM][$DiEtSO_4$] across 298–333 K, which may partly account for the differences in their SO_2 absorption behavior. Overall, these findings suggest that [MIM][$DiEtSO_4$] holds promise as a viable candidate for SO_2 separation applications.

Table 1
Properties and SO_2 uptake capacity of $DiEtSO_4$-based ILs at 1 bar and 298 K.

Entry	$DiEtSO_4$-based ILs	Density/ (g/cm^3)	Viscosity/ cP	SO_2 uptake capacitys/ (mmol/g)	H_m/ (kPa·kg/ mol)
1	[Py][$DiEtSO_4$]	1.26733	19.60	5.61	18.46
2	[BiPy][$DiEtSO_4$]	1.26051	284.42	9.34	12.67
3	[MIM][$DiEtSO_4$]	1.23581	57.96	9.57	13.40
4	[TEA][$DiEtSO_4$]	1.22058	3.13	3.22	22.57
5	[DBU][$DiEtSO_4$]	1.18728	210.93	9.69	13.42

Furthermore, SO_2 absorption kinetics of two representative ILs ([MIM][$DiEtSO_4$] and [DBU][$DiEtSO_4$]) were analyzed at 298–313 K to evaluate the relationship between absorption temperature, SO_2 absorption rate, and SO_2 equilibrium uptake (Fig. 2e). The results show that the selected $DiEtSO_4$-based ILs reach their maximum SO_2 uptake within 2.5 min. Meanwhile, total SO_2 uptakes by [MIM][$DiEtSO_4$] and [DBU][$DiEtSO_4$] decrease with increasing temperature, which indicates that higher temperatures suppress SO_2 absorption, reflecting a shift in gas-liquid equilibrium toward the gas phase and a reduced solubility of SO_2 in the IL phase. Besides, [MIM][$DiEtSO_4$] exhibited a significantly higher SO_2 absorption efficiency than [DBU][$DiEtSO_4$] at 298 K (8.03 *vs.* 5.29 mmol/g within 1 min), reaching 84% of its full capacity. At 298 K, the reduced SO_2 absorption rate of [DBU][$DiEtSO_4$] is attributed to its higher initial viscosity (210.93 cP), and the subsequent viscosity increase during absorption, which imposes kinetic constraints on SO_2 diffusion within the IL phase. However, these limitations are mitigated as the absorption temperatures increased to 303 K and 313 K, resulting in acceleration of SO_2 absorption rate for [DBU][$DiEtSO_4$] within 1 min, which is higher than that of 298 K. It should be noted that [DBU][$DiEtSO_4$] exhibits highest SO_2 uptake (6.8 g/mmol) within 1 min at 303 K, which reflects an optimal compromise between SO_2 absorption kinetics and thermodynamics. In short, these results suggest that elevated temperature promotes diffusion but also encounters a trade-off with decreased solubility, which is consistent with the observed decreasing SO_2 saturation plateau.

3.2. DFT and COSMOtherm analysis

The molecular ESP analysis provides a three-dimensional view of charge distribution, which helps to identify regions where electrophilic or nucleophilic interactions are likely to occur. ESP maps of $DiEtSO_4$-based ILs and SO_2 were obtained by DFT (Fig. 3a–f), and the proportions of areas corresponding to different ESP intervals are summarized in

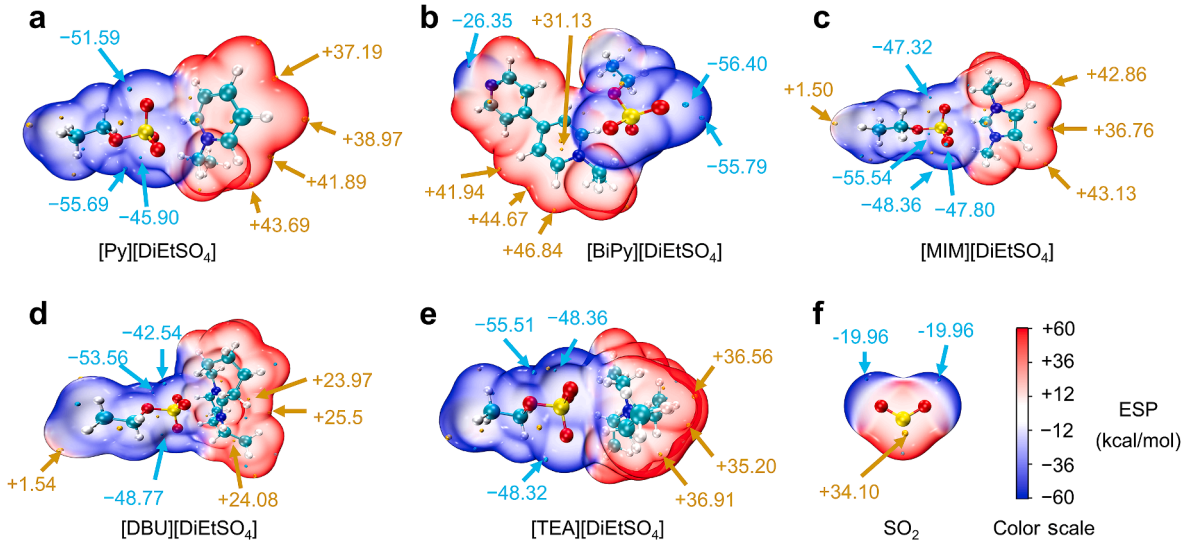

Fig. 3. Optimized geometry structures and surface electrostatic potential maps of (a) [Py][$DiEtSO_4$], (b) [BiPy][$DiEtSO_4$], (c) [MIM][$DiEtSO_4$], (d) [DBU][$DiEtSO_4$], (e) [TEA][$DiEtSO_4$], and (f) SO_2.

Fig. S13. The results show that the anionic $[DiEtSO_4]^-$ moiety exhibits pronounced negative potential regions, primarily localized around the oxygen atoms of the sulfate group. The cationic moieties display positive potential regions of varying magnitude, which are associated with electropositive hydrogen atoms or electron-deficient carbon centers. Notably, the cationic side of [BiPy][$DiEtSO_4$] shows a moderately attenuated negative potential (−26.35 kcal/mol) compared to [Py][$DiEtSO_4$], suggesting that the extended π-conjugation effect in $[BiPy]^+$ cations delocalizes the positive charge and reduces localized electrophilicity (Fig. 3a–b). In addition, weak positive regions (1.50 *vs.* 1.54 kcal/mol) are observed around the single-bonded carbon atoms of the anions in [MIM][$DiEtSO_4$] and [DBU][$DiEtSO_4$], and these subtle positive patches may arise from *σ*-hole effects (Fig. 3c and 3d). The positive charge region (~36 kcal/mol) of [TEA][$DiEtSO_4$] shows relatively small fluctuation among the five ILs, suggesting a more uniform electrostatic environment around its cation (Fig. 3e). Additionally, SO_2 shows a highly polarized structure, with the sulfur atom possessing a strong positive potential (+34.10 kcal/mol) and both oxygen atoms having negative potential (−19.96 kcal/mol), suggesting its ability to engage in electrostatic interactions with electron-rich sites in $DiEtSO_4$-based ILs (Fig. 3f). Therefore, these findings suggest that electron-deficient SO_2 molecules absorbed by $DiEtSO_4$-based ILs are likely to be located in the interionic space between ion–ion pairs.

The *σ*-profile curve reflects the variation in the probability $p(\sigma)$ and chemical potential $\mu(\sigma)$ of the molecular surface charge distribution as a function of the surface charge density [38]. In this work, the COSMOtherm calculations were employed to obtain surface charge density distributions (Fig. 4a), *σ*-profiles (Fig. 4b), and chemical potentials (Fig. 4c) of the components within the investigated $DiEtSO_4$-based ILs system. Based on the features of *σ* values, three distinct regions can be defined: the nonpolar region, corresponding to *σ* values within ±0.0084 e/Å^2; the hydrogen-bond acceptor (HBA) and the hydrogen-bond donor (HBD) regions on the positive and negative ±0.0084 e/Å^2 side, respectively [39]. The *σ*-profiles of $DiEtSO_4$-based ILs exhibit relatively broad

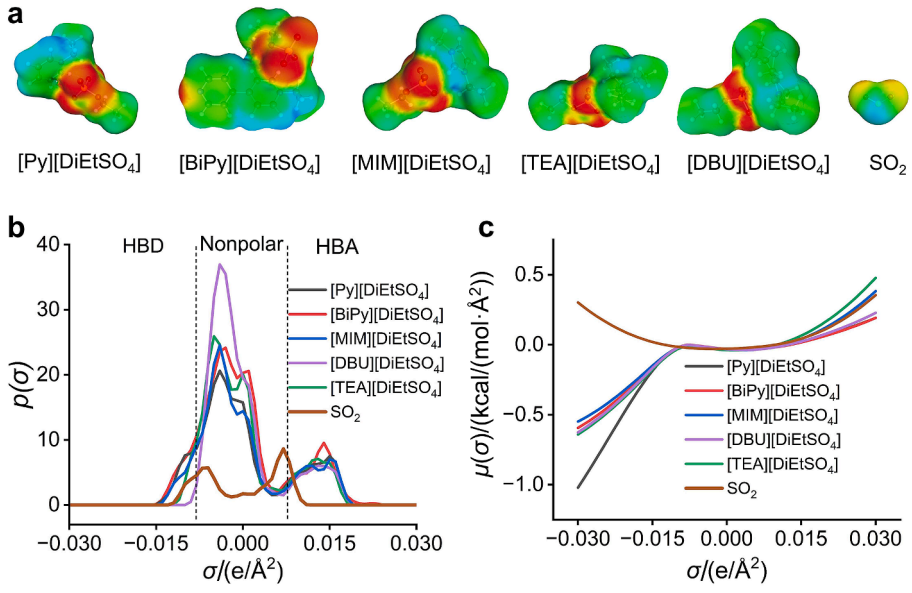

Fig. 4. (a) Surface charge density distributions, (b) *σ*-profile, and (c) chemical potential $\mu(\sigma)$ analysis of $DiEtSO_4$-based ILs and SO_2.

distributions, with dominant contributions in the nonpolar and HBA regions (Fig. 4b). In contrast, SO_2 is largely confined to the nonpolar region. Specifically, its sulfur atoms give rise to a pronounced positive peak at $\sigma = +0.0071$ e/Å^2, whereas the two polar oxygen atom produces a distinct negative peak at $\sigma = -0.0066$ e/Å^2. This distribution pattern suggests the presence of weak hydrogen-bonding interactions between SO_2 and $DiEtSO_4$-based ILs. Moreover, the variation in chemical potential for SO_2 in the negatively charged region deviates markedly from that of $DiEtSO_4$-based ILs, which supports that the selected anions have negligible effects on the SO_2 absorption performance. Besides, Fig. 4c shows that the chemical potential distributions of SO_2 and $DiEtSO_4$--based ILs are mainly concentrated in the nonpolar region, indicating that SO_2 absorption in these ILs is governed predominantly by physical rather than chemical interactions.

To further evaluate the nature and strength of the interactions between $DiEtSO_4$-based ILs and SO_2, IGM was employed to visualize inter- and intra-fragment interactions *via* isosurface analysis (Fig. 5). It can be found that SO_2 resides at the periphery of $DiEtSO_4$-based ILs and the surrounding isosurface appears pure green, indicating that van der Waals interactions dominate SO_2 absorption. On the other hand, the location of SO_2 between the cation-anion pairs gives rise to tiny blue green isosurface patches, without any distinct repulsive regions. Moreover, it is worth noting that substitution of the $[Py]^+$ cation with $[BiPy]^+$ generates a localized blue attractive region in the SO_2 + $[BiPy][DiEtSO_4]$ system, which is attributed to the π-conjugation of $[BiPy]^+$ structure and the electron-donating property of the ethyl substituent (Fig. 5a–b). This result suggests that $[BiPy][DiEtSO_4]$ enhances SO_2 absorption *via* electrostatic interactions and Coulombic attraction, resulting in nonlinear SO_2 absorption in the low-pressure region (Fig. 2c). For SO_2 + $[MIM][DiEtSO_4]$ binary system, Fig. 5c reveals that only weak van der Waals interactions are evident. Similarly, the two blue green isosurfaces between sulfur and oxygen atoms reveal the coexistence of van der Waals and electrostatic attractions in both SO_2 + $[TEA][DiEtSO_4]$ and SO_2 + $[DBU][DiEtSO_4]$ systems, which supports that their SO_2 absorption patterns are governed by non-covalent interactions rather than strong chemical bonds (Fig. 5d–5e). Overall, these findings show that the absorptive interactions identified are in excellent agreement with σ-profile and ESP analysis. Furthermore, the results also demonstrate that cation structure modulation can effectively change the electronic density distribution of ILs, allowing for molecular-level tuning of the interaction between SO_2 and ILs.

3.3. SO_2 absorption behavior and thermodynamics

The pressure and temperature dependence of SO_2 uptake was analyzed for $DiEtSO_4$-based ILs, as shown in Figs. 6a–6b and S14. It can be found that the SO_2 absorption capacity of $DiEtSO_4$-based ILs increases with rising pressure at 298–313 K, whereas elevated temperatures tend to reduce SO_2 capacity. Moreover, SO_2 absorption isotherms of $[TEA][DiEtSO_4]$ and $[Py][DiEtSO_4]$ exhibit consistent physical absorption behavior. The chemical adsorption ratios of SO_2 for $[MIM][DiEtSO_4]$, $[DBU][DiEtSO_4]$, and $[BiPy][DiEtSO_4]$ are negligible within 0–0.2 bar. Therefore, their SO_2 adsorption processes can be reasonably classified as physical adsorption. These results mean that $DiEtSO_4$-based ILs for SO_2 absorption is an exothermic process and aligns with classical Henry's law [40]. Furthermore, to streamline the experimental procedure, the representative ILs $[MIM][DiEtSO_4]$ and $[DBU][DiEtSO_4]$ were selected for subsequent investigations. As shown in Fig. 6c–d, SO_2 absorption isotherms are fitted with the Henry's law model ($R^2 > 0.99$, Eq. (1)), and the calculated Henry constants (H_m) were 13.40 kPa·kg/mol ($[MIM][DiEtSO_4]$) and 13.42 kPa·kg/mol ($[DBU][DiEtSO_4]$), respectively (Table 1). Besides, the excellent *P*-values ($P < 0.05$) indicate a reliable fit to the experimental data, which confirms that the SO_2 uptake mechanism is simple, solubility-controlled in $DiEtSO_4$-based ILs. Additionally, the Fourier transform infrared spectroscopy (FT-IR) spectra of the fresh and SO_2-loaded samples were largely similar. Specifically, the identifiable stretching vibration peaks within the 1316–945 cm^{-1} region, corresponding to the S═O and S–O bonds of $DiEtSO_4$, showed no observable redshift (Fig. 6e–f) [15]. This result suggests that the interaction between SO_2 molecules and $[MIM][DiEtSO_4]$ and $[DBU][DiEtSO_4]$ is governed solely by physical dissolution rather than chemical bonding. Therefore, the above findings demonstrate that $DiEtSO_4$-based

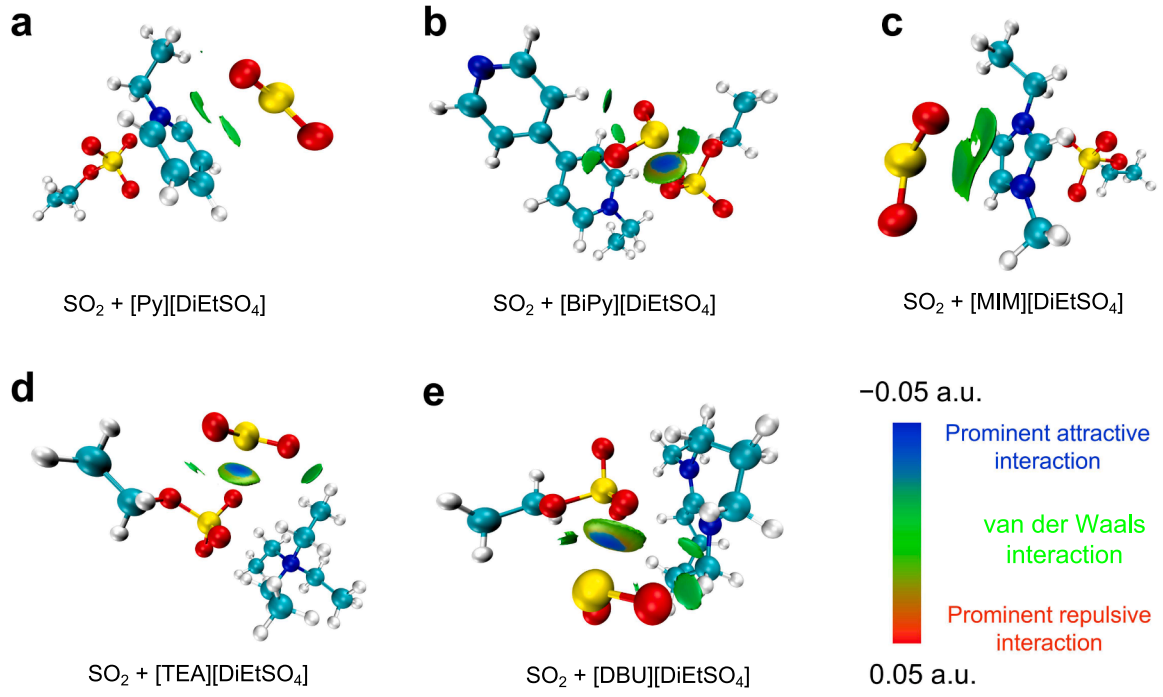

Fig. 5. Weak interaction analysis of specific inter- and intra-fragment interactions between SO_2 and $DiEtSO_4$-based ILs based on the Hirshfeld partition of molecular density (isovalue = 0.01 a.u., surface sign = −0.05–0.05 a.u.).

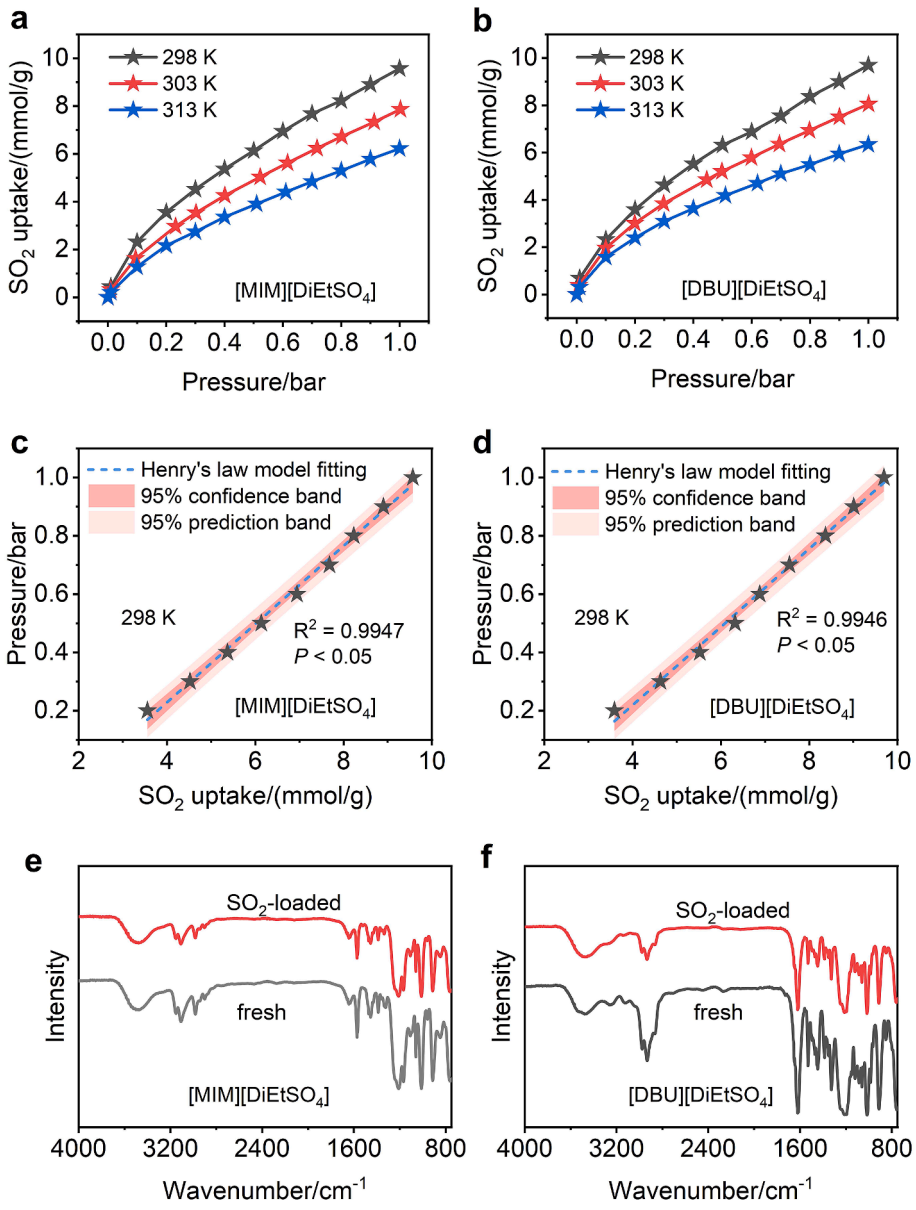

Fig. 6. (a–b) SO_2 adsorption isotherms of [MIM][$DiEtSO_4$] and [DBU][$DiEtSO_4$] at 298–313 K and 1 bar; (c–d) Henry and Pearson correlation coefficients between SO_2 uptake and absorption pressure for [MIM][$DiEtSO_4$] and [DBU][$DiEtSO_4$]; (e–f) FT-IR spectra of fresh and SO_2-loaded [MIM][$DiEtSO_4$] and [DBU][$DiEtSO_4$].

ILs have strong adherence to Henry's law behavior under the tested conditions.

Henry's law constant H_m (T, P) is defined by the following expression:

$$H_m(T,P) = \lim_{m_{SO_2}\to 0} \frac{f^g}{m_{SO_2}} \approx \frac{P}{m_{SO_2}} \quad (1)$$

Where H_m is the Henry's law constant, with units of kPa·kg/mol; f^g represents the fugacity of SO_2 in the gas phase; m_{SO_2} is the molal concentration of SO_2 dissolved in the liquid phase (mol/kg); P denotes the partial pressure of SO_2 in $DiEtSO_4$-based ILs.

Based on the preceding analysis, H_m of $DiEtSO_4$-based ILs at 298–313 K were calculated using the Henry's law model (Eq. (1)), and the results were shown in Fig. S15. It can be observed that $DiEtSO_4$-based ILs exhibit increasing H_m values with temperature, which implies reduced SO_2 uptake at rising temperature conditions. This trend is consistent with the exothermic nature of the physical absorption process, as expected by thermodynamics. In addition, the H_m value of [TEA][$DiEtSO_4$] rose sharply from 22.57 kPa·kg/mol to 66.03 kPa·kg/mol at 298–313 K, which may be attributed to the entropy increase caused by the lower viscosity and weaker electrostatic interactions at higher temperatures. The relationship between the adsorption equilibrium constants (K) and temperatures could be described by Eq. (2) [40]. Furthermore, to ensure the reliability of the calculated enthalpy changes (ΔH), the SO_2 absorption isotherms of [MIM][$DiEtSO_4$] and [DBU][$DiEtSO_4$] were also measured at 323–333 K and 1 bar (Fig. S16), expanding the initial temperature range of 298–313 K. (Fig. 6a and 6b). The fitting results show good linearity ($R^2 > 0.98$), supporting the validity of Henry's law over the tested temperature ranges (Fig. 7). The calculated ΔH values for [MIM][$DiEtSO_4$] (−19.08 kJ/mol) and [DBU][$DiEtSO_4$] (−18.18 kJ/mol) are below the commonly accepted chemisorption threshold value of 40 kJ/mol, which confirms that SO_2 absorption by $DiEtSO_4$-based ILs *via* a moderate exothermic physical absorption mechanism. In short, H_m profiles and thermomechanical analyses confirm that SO_2 absorption in $DiEtSO_4$-based ILs is dominantly governed by temperature-dependent solubility, with negligible chemical

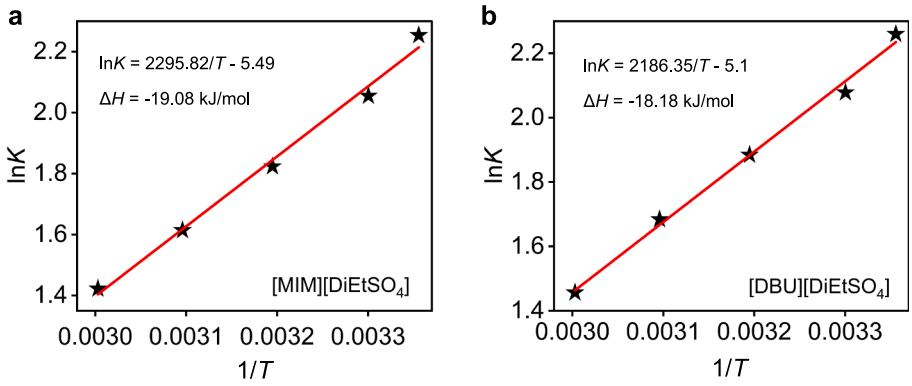

Fig. 7. Linear fit of equilibrium constant (ln$K$) and $1/T$ for SO_2 adsorption in (a) [MIM][DiEtSO$_4$] and (b) [DBU][DiEtSO$_4$].

interaction, as further corroborated by FT-IR. As a result, the gas-liquid mass transfer model applies to DiEtSO$_4$-based ILs to study the k_La and k_L in relation to viscosity and SO_2 absorption capacity.

$$\frac{\partial \ln K}{\partial(1/T)} = -\frac{\Delta H}{R} \tag{2}$$

Where T is the adsorption temperature (K), R is the universal gas constant (8.314 J/(mol·K)).

3.4. Liquid side mass transfer coefficients

k_La and k_L are important technical parameters describing the efficiency of the mass transfer process between gas and liquid and are essential for the correct design and operation of industrial absorption apparatus [25,26]. Gas-liquid mass transfer during physical absorption is commonly described by the film theory. This theory assumes the existence of a stagnant boundary layer at the gas-liquid interface, across which gas molecules diffuse into the liquid phase [41]. Therefore, to quantitatively evaluate the mass transfer characteristics of SO_2 in DiEtSO$_4$-based ILs, the gas-liquid mass transfer models (Eqs. (3) and (4)) were employed to determine k_La and k_L values, with the corresponding results are summarized in Fig. 8 and Table 2. In addition, the relevant equations for calculation and derivation (Eqs. (S4)-(S7)) are described in Supporting Information.

Table 2
The calculated k_La and k_L values of DiEtSO$_4$-based ILs at 298 K.

Entry	DiEtSO$_4$-based ILs	$k_La \times 10^3/s^{-1}$	$k_L/(\times 10^6$ m/s)
1	[TEA][DiEtSO$_4$]	4.98	4.53
2	[Py][DiEtSO$_4$]	2.41	2.19
3	[MIM][DiEtSO$_4$]	1.07	0.97
4	[DBU][DiEtSO$_4$]	0.69	0.63
5	[BiPy][DiEtSO$_4$]	0.47	0.43

$$k_La \cdot t = \frac{\beta}{1+\beta} \cdot \ln\left(\frac{P^m_{SO_2}}{(1+\beta)\cdot P_{SO_2}(t) - \beta \cdot P^m_{SO_2}}\right); \text{ with } \beta = \frac{V_G}{V_{IL}\cdot R\cdot T\cdot H_{SO_2}} \tag{3}$$

Where k_La is volumetric liquid-side mass transfer coefficient (s^{-1}), t is the absorption time (s), and $P^m_{SO_2}$ represent the initial partial pressure and the transient partial pressure (Pa) of SO_2 at time t, respectively. β is a dimensionless parameter, and V_G and V_{IL} denote the volumes of the gas phase and the ionic liquid (m^3), H_{SO_2} is the Henry's law constant (kPa·kg/mol).

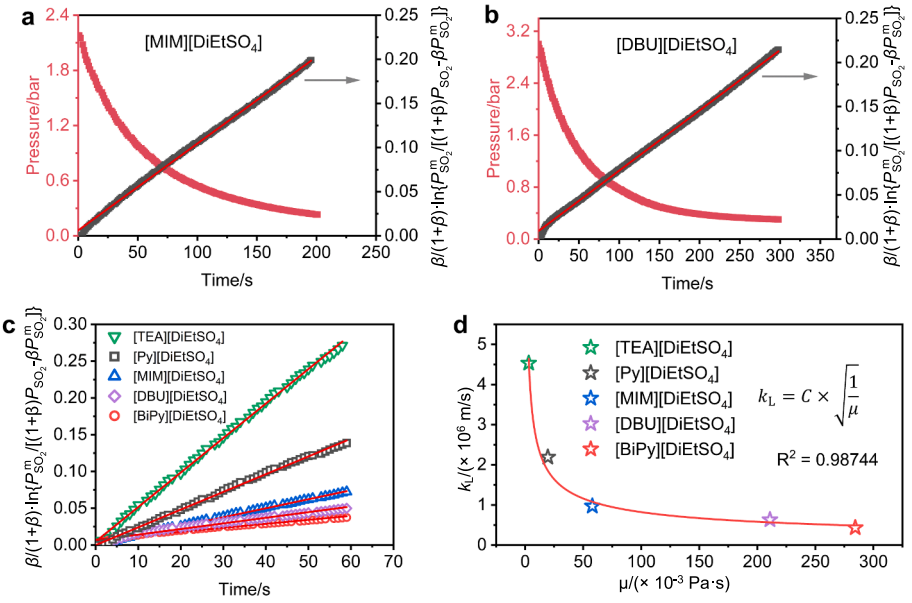

Fig. 8. Determination of k_La from SO_2 absorption experiments at 298 K for (a) [MIM][DiEtSO$_4$] and (b) [DBU][DiEtSO$_4$]; (c) determination of k_La in DiEtSO$_4$-based ILs; (d) the relationship between k_L and μ.

$$k_L = \frac{k_L a}{a} \quad (4)$$

Where k_L is liquid-side mass transfer coefficient (m/s), and a is specific gas-liquid interfacial area (m^2/m^3).

The value of $k_L a$ is obtained by linear regression of the transformed pressure data, where the ordinate is defined by Eq. (S3) and the abscissa is time (t). k_L is subsequently calculated by dividing $k_L a$ by the interfacial area a (9.1×10^2 m^2/m^3). As shown in Fig. 8a–b, the temporal profiles of pressure and $k_L a$ in [MIM][DiEtSO$_4$] and [DBU][DiEtSO$_4$] were obtained by the pressure drop method. The observed steady declines in pressure reflect continuous SO_2 uptake into the DiEtSO$_4$-based ILs phase. Concurrently, the corresponding $k_L a$ increases linearly, which suggests that the mass transfer rate is consistent before approaching SO_2 adsorption equilibrium, and $k_L a$ values are calculated as the slope of the linear fit to the experimental data. Subsequently, the same experimental protocol was used to determine $k_L a$ values of the other three DiEtSO$_4$-based ILs (Fig. 8c and Table 2). To ensure data comparability, the initial absorption interval of 0–60 s was selected for analysis, as this period exhibits consistent kinetic behavior and is minimally influenced by external perturbations. As anticipated, the cationic structures of DiEtSO$_4$-based ILs exert a significant impact not only on their SO_2 adsorption performance and bulk viscosity but also on the overall $k_L a$. Notably, the observed variation trends in $k_L a$ values exhibit a clear correlation with the viscosities of the respective DiEtSO$_4$-based ILs (Fig. 2b). These trends are consistent with previous studies on the use of ILs for gas capture, wherein μ has been identified as a critical factor influencing mass transfer efficiency [9,26]. Furthermore, consistent with prior analysis of DiEtSO$_4$-IL cation structure, SO_2 dissolved in the IL phase occupies the electrostatic potential wells between ions. The extent to which absorption alters μ is strongly governed by the specific configuration of the ion pairs. Therefore, it is reasonable to infer that k_L is likewise influenced by the structural attributes of DiEtSO$_4$-based ILs.

Furthermore, to elucidate the controlling factors in k_L, the surface renewal theory proposed by Danckwerts was employed to establish a quantitative relationship between k_L and μ of DiEtSO$_4$-based ILs. According to this theory, the gas-liquid interface is continuously refreshed by bulk liquid motion, forming a dynamic boundary layer that facilitates the diffusion of gas molecules into the liquid phase [27,42]. Based on this framework, the liquid-side mass transfer coefficient is expressed as:

$$k_L = \sqrt{D_R S} \quad (5)$$

where D_R represents the diffusivity of the gas in DiEtSO$_4$-based ILs, and S is the surface renewal frequency. Incorporating the empirical expression for D_R:

$$D_R = 7.4 \times 10^{-8} \frac{T\sqrt{\phi M}}{\mu V_R^{0.6}} \quad (6)$$

where φ is the association factor of ILs, M is the molecular weight of SO_2 gas (g/mol), $V_R^{0.6}$ is the molar volume of ILs at its normal boiling point (cm^3/mol).

The model simplifies to:

$$k_L = C \times \sqrt{\frac{1}{\mu}} \quad (7)$$

where C is the model constant.

As shown in Tables 1 and 2, the calculated k_L values exhibit a clear inverse correlation with μ of DiEtSO$_4$-based ILs ($R^2 > 0.98$). For instance, [TEA][DiEtSO$_4$] has the lowest μ (3.13×10^{-3} Pa·s) among the tested ILs, exhibits the highest k_L value (4.53×10^6 m/s), whereas [Bipy][DiEtSO$_4$] with the highest μ (284.42×10^{-3} Pa·s) shows a significantly lower k_L value (0.43×10^6 m/s). This inverse trend aligns well with the model predictions, reinforcing the dominant role of μ in governing liquid-phase mass transfer. In addition, the model constant C value was determined to be 9.03, falling within the expected range of 2–15, which supports the validity of the proposed model in describing μ-dependent behavior of k_L across DiEtSO$_4$-based ILs systems. Therefore, the results confirm the applicability of the surface renewal theory with respect to mass transfer phenomena during the absorption process of DiEtSO$_4$-based ILs. In addition, lower μ facilitates enhanced SO_2 absorption efficiency within the IL phase, as evidenced in Fig. 2e. Therefore, IL systems with viscosities less than or equal to 60 cP ($\mu \leq 60 \times 10^{-3}$ Pa·s) are recommended to achieve efficient SO_2 absorption and mass transfer performance.

3.5. Applicability

In industrial waste gas treatment, the selectivity of absorbents for the guest absorbent is an important basis for their applicability. The CO_2 absorption isotherms of DiEtSO$_4$-based ILs were measured at 298 K and 1 bar, and the selectivity of SO_2/CO_2 under different SO_2 mole fractions in the gas phase was calculated using the ideal adsorbed solution theory (IAST). The results indicated that the CO_2 adsorption behavior in DiEtSO$_4$-based ILs exhibited a linear trend with CO_2 uptake capacities below 0.23 mmol/g, which implies that CO_2 uptake was carried out *via* physical dissolution with low affinity (Fig. S17). In addition, IAST calculations revealed the SO_2/CO_2 selectivity sequence among the ILs as follows: [MIM][DiEtSO$_4$] > [Bipy][DiEtSO$_4$] > [DBU][DiEtSO$_4$] > [Py][DiEtSO$_4$] > [TEA][DiEtSO$_4$] (Fig. 9a). Notably, [MIM][DiEtSO$_4$] demonstrated satisfactory IAST SO_2/CO_2 selectivity (up to 183.26) at 298 K and 1 bar, outperforming many conventional ILs and DES absorbents, which typically show IAST SO_2/CO_2 selectivity below 100. Furthermore, the reusability of [MIM][DiEtSO$_4$] was validated in ten consecutive absorption-desorption cycles, with negligible capacity loss. The results support the dual advantage of [MIM][DiEtSO$_4$] in achieving

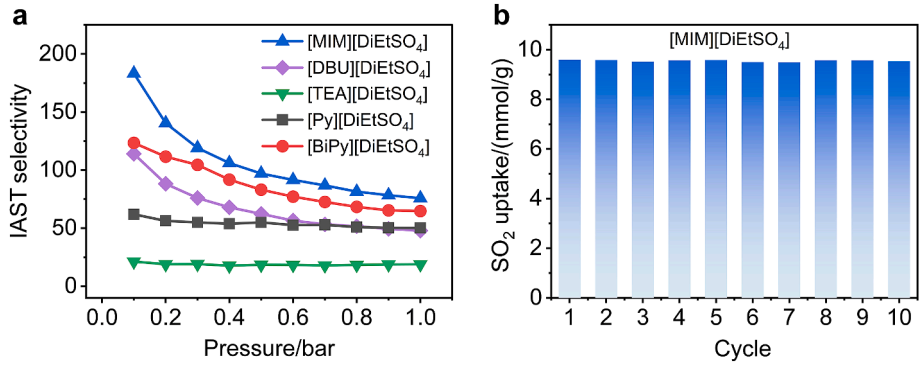

Fig. 9. (a) IAST selectivity of SO_2/CO_2 at 298 K and 1 bar; (b) the recovered [MIM][DiEtSO$_4$] for SO_2 absorption at 298 K and 1 bar.

Table 3
SO_2 uptake rates and capacities of $DiEtSO_4$-based ILs and various absorbents reported in the literature.

Entry	Absorbents	T/K	P/bar	Saturated-SO_2 uptake time/min	Saturated-SO_2 uptake capacity	Reuptake capacity loss, %	Ref
1	$[P_{4442}][FA]$	303	1	< 30	0.56 g/g (8.75 mmol/g)	3.61	[44]
2	$[P_{4442}][TFSI]$	293	1	~13	4.27 mol/mol (9.45 mmol/g)	11.71	[16]
3	$[P_{66614}][4\text{-PyO}]$	293	1	~25	6.00 mol/mol (10.40 mmol/g)	11.53	[45]
4	[Na(PEG400)][Tetz]	303	0.2	< 6	0.93 mol/mol (1.89 mmol/g)	13.64	[46]
5	$[P_{66614}][BenIm]$	293	1	< 10	5.75 mol/mol (9.58 mmol/g)	17.91	[11]
6	Mat-MAA (1:2)	293	1	~3.5	0.81 g/g (12.66 mmol/g)	14.81	[15]
7	L-car + EG (1:3)	313	1	~60	0.37 g/g (5.78 mmol/g)	13.51%	[17]
8	Im-Gly (1:2)	313	0.02	< 175	0.16 g/g (2.50 mmol/g)	34.14	[47]
9	$[DBU][DiEtSO_4]$	298	1	< 2.5	9.69 mmol/g	~0.1	This work
10	$[MIM][DiEtSO_4]$	298	1	< 2	9.57 mmol/g	~0.1	This work

Note: $[P_{4442}][FA]$: tributylethylphosphonium 2-furoic acid; $[P_{4442}][TFSI]$: tributylethylphosphonium bis(trifluoromethylsulfonyl)imide; $[P_{66614}][4\text{-PyO}]$: hexyltetradecylphosphonium 4-pyridinol; [Na(PEG400)][Tetz]: sodium poly(ethvlene alvco)400 1H-tetrazole; $[P_{66614}][BenIm]$: hexyltetradecylphosphonium benzimidazole; Mat-MAA: matrine N-methylacetamide; L-car: L-carnitine; EG: ethylene glycol; Im-Gly: imidazole glycerol; $[DBU][DiEtSO_4]$: 1,8-diazabicyclo[5.4.0]undec-7-ene diethyl sulfate; $[MIM][DiEtSO_4]$: 1-methylimidazole diethyl sulfate.

efficient SO_2/CO_2 separation while maintaining excellent operational stability.

Furthermore, the reversibility and durability of the absorbents are indicators of their practical applicability [12,43]. Fig. 9b and S18 show SO_2 absorption performance of $[MIM][DiEtSO_4]$ and $[DBU][DiEtSO_4]$ over ten successive cycles at 298 K and 1 bar. The results show that $[MIM][DiEtSO_4]$ and $[DBU][DiEtSO_4]$ demonstrate excellent reusability and stability, with SO_2 uptake consistently maintained at ~9.6 mmol/g. The negligible fluctuation in SO_2 uptake capacities suggests that $DiEtSO_4$-based ILs retain their structural integrity throughout the absorption-desorption cycles. Besides, the structural differences between $[MIM][DiEtSO_4]$ and $[DBU][DiEtSO_4]$ do not appear to compromise their recyclability, which implies that $DiEtSO_4$-based ILs are well-suited for long-term SO_2 separation applications. In addition, the comparison between $[MIM][DiEtSO_4]$, $[DBU][DiEtSO_4]$, and the reported absorbents for SO_2 absorption was summarized in Table 3. It can be observed that $[MIM][DiEtSO_4]$ and $[DBU][DiEtSO_4]$ exhibit several notable advantages over previously reported SO_2 separation. On the one hand, both $[MIM][DiEtSO_4]$ and $[DBU][DiEtSO_4]$ achieve exceptionally rapid SO_2 uptake (~9.6 mmol/g) within 2.5 min, which is faster than most IL- and DES-type absorbents whose saturation times typically range from 10 to 60 min. On the other hand, $[MIM][DiEtSO_4]$ and $[DBU][DiEtSO_4]$ have excellent cycling stability, with negligible SO_2 capacity loss (only ~0.1%) after repeated absorption-desorption cycles, which is much less than the level of capacity loss (~10%–30%) of comparable systems. Therefore, these results demonstrate that $DiEtSO_4$-based ILs are promising sustainable sorbents for the efficient separation and purification of waste SO_2 from industrial exhaust gas.

4. Conclusions

In summary, we successfully synthesized five $DiEtSO_4$-based ILs with controlled cationic structures, achieving viscosities spanning 3–285 cP. The physicochemical properties, SO_2 absorption performance, and mass transfer behavior of $DiEtSO_4$-based ILs were investigated to elucidate the relationship between μ and gas-liquid mass transfer efficiency. The results demonstrated that μ plays a key role in governing both the absorption kinetics and k_L of SO_2 in $DiEtSO_4$-based IL systems. Among the five ILs studied, $[MIM][DiEtSO_4]$ exhibited superior SO_2 uptake capacities (~9.6 mmol/g), excellent IAST selectivity (183.26) and favorable mass transfer characteristics (8.03 mmol/g within 1 min, 0.97×10^6 m/s), with the smallest μ change upon SO_2 absorption (~11%) at 298 K. Furthermore, DFT, COSMOtherm, and thermodynamic analysis confirmed that SO_2 uptake in these ILs is governed by physical dissolution, with negligible chemical interaction (ΔH < ~19 kJ/mol), as evidenced by similar FT-IR spectra before and after absorption. Notably, the determined k_L values revealed a clear inverse correlation between μ and k_L, consistent with predictions from the Danckwerts theory. Meanwhile, the established quantitative correlation shows that $k_L \propto \mu^{-0.5}$, which not only validates the applicability of this theory to $DiEtSO_4$-based ILs but also offers a predictive basis for designing ILs with optimized viscosity. Accordingly, $DiEtSO_4$-based ILs systems with $\mu \leq 60$ cP are identified as more suitable for achieving efficient SO_2 absorption and mass transfer efficiency. Additionally, the excellent recyclability of $[MIM][DiEtSO_4]$ and $[DBU][DiEtSO_4]$ over ten cyclic tests further supports their potential for sustainable and efficient SO_2 capture in industrial applications.

CRediT authorship contribution statement

Wei Hui: Writing – review & editing, Writing – original draft, Investigation, Funding acquisition, Formal analysis. **Xin Wang:** Visualization, Investigation, Formal analysis. **Xiao-Ya Wang:** Investigation. **Fei-Feng Mao:** Validation, Software. **Tiao Zhang:** Methodology, Investigation. **Yan Zhou:** Resources, Investigation, Formal analysis. **Jia-Yin Zhang:** Supervision, Investigation. **Duan-Jian Tao:** Writing – original draft, Resources, Funding acquisition, Conceptualization.

Declaration of competing interests

The authors declare that they have no known competing financial interests or personal relationships that could have appeared to influence the work reported in this paper.

Acknowledgments

We gratefully thank the National Natural Science Foundations of China (22378178), the Natural Science Foundations of Jiangxi Province (20242BAB20111), the Natural Science Foundation of Ji'an (20244–018658), and the Key Laboratory of Jiangxi Province for Functional Biology and Pollution Control in Red Soil Regions (2023SSY02051) for financial support.

Appendix A. Supplementary data

Supplementary data to this article can be found online at https://doi.org/10.1016/j.gce.2025.12.005.

Nomenclature

ILs	Ionic liquids	μ	Viscosity, cP or $\times 10^{-3}$ Pa·s
DESs	Deep eutectic solvents	ρ	Density, g/cm^3
SO_2	Sulfur dioxide	k_La	Volumetric mass transfer coefficient, s
CO_2	Carbon dioxide	a	Interfacial area, m^2/m^3
$DiEtSO_4$	Diethyl sulfate	k_L	Mass transfer coefficient, m/s
BiPy	4,4-Bipyridine	T	Temperature, K
DBU	1,8-Diazabicyclo[5.4.0]undec-7-ene diethyl sulfate	t	Time, s
TEA	Triethylamine	V	Volume, m^3
Py	Pyridine	σ	Surface charge density, e/Å^2
MIM	Methylimidazole	$\mu(\sigma)$	Chemical potential function of σ, kcal/(mol·Å^2)
HBA	Hydrogen bond acceptor	$p(\sigma)$	Probability function of σ
HBD	Hydrogen bond donor	ΔH	Absorption enthalpy, kJ/mol
IAST	Ideal adsorbed solution theory	K	Absorption equilibrium constant
DFT	Density functional theory	H_m	Henry's law constant, kPa·kg/mol
IGM	Independent gradient model	f^g	Fugacity of gas in the gas phase
IGMH	IGM based on Hirshfeld partition of molecular density	M	Molecular weight, g/mol
ESP	Electrostatic potential	D_R	Diffusion coefficient, m^2/s
		ϕ	Association factor

References

[1] S. Yan, F. Han, Q. Hou, S. Zhang, S. Ai, Recent advances in ionic liquid-mediated SO_2 capture, Ind. Eng. Chem. Res. 58 (2019) 13804–13818.
[2] H. Wang, P. Wu, C. Li, J. Zhang, R. Deng, Reversible and efficient absorption of SO_2 with natural amino acid aqueous aolutions: performance and mechanism, ACS Sustainable Chem. Eng. 10 (2022) 4451–4461.
[3] Y.-N. Dong, W.-C. Chen, L.-L. Zhang, B.-C. Sun, G.-W. Chu, J.-F. Chen, Kinetic study of SO_2 with sodium lactate based deep eutectic solvents and modelling of desulfurization intensification in rotating packed bed reactor, Chem. Eng. Sci. 248 (2022) 117197.
[4] W. Xiao, J.-Q. Chen, J. Wu, Radical sulfonylation with sulfur dioxide surrogates, Chem. Soc. Rev. 54 (2025) 6832–6926.
[5] P. Vogel, M.r. Turks, L. Bouchez, D. Marković, A. Varela-Álvarez, J.Á. Sordo, New organic chemistry of sulfur dioxide, Acc. Chem. Res. 40 (2007) 931–942.
[6] M. Kim, C.E. Obertone, C.B. Kelly, C.A. Reiher, C. Grosanu, J.C. Robertson, M. D. Levin, Accessing sulfonamides *via* formal SO_2 insertion into C–N bonds, Nat. Chem. 17 (2025) 1247–1255.
[7] Our world in data, global sulphur dioxide (SO_2) emissions by world region. https://ourworldindata.org/grapher/so-emissions-by-world-region-in-million-tonnes, 2025 (accessed 27 January 2026).
[8] R. Faiz, K. Li, Olefin/paraffin separation using membrane based facilitated transport/chemical absorption techniques, Chem. Eng. Sci. 73 (2012) 261–284.
[9] S. Asensio-Delgado, F. Pardo, G. Zarca, A. Urtiaga, Absorption separation of fluorinated refrigerant gases with ionic liquids: equilibrium, mass transport, and process design, Sep. Purif. Technol. 276 (2021) 119363.
[10] S. Ren, Y. Hou, K. Zhang, W. Wu, Ionic liquids: functionalization and absorption of SO_2, Green Energy Environ. 3 (2018) 179–190.
[11] G. Cui, W. Lin, F. Ding, X. Luo, X. He, H. Li, C. Wang, Highly efficient SO_2 capture by phenyl-containing azole-based ionic liquids through multiple-site interactions, Green Chem. 16 (2014) 1211–1216.
[12] S. Zhang, J. Sun, X. Zhang, J. Xin, Q. Miao, J. Wang, Ionic liquid-based green processes for energy production, Chem. Soc. Rev. 43 (2014) 7838–7869.
[13] H. Ning, M. Shi, Q. Yang, J. Huang, X. Zhang, Y. Wu, K. Jie, Rational design of porous ionic liquids for coupling natural gas purification with waste gas conversion, Angew. Chem. Int. Ed. 62 (2023) e202310741.
[14] Z. Xu, S. Wen, Q. Zhao, C. Zhao, K. Huang, X. Zhang, L. Zheng, K. Jie, Y. Wu, Porous ionic liquids featuring chemical site toward low-rressure CO_2 capture and conversion, Adv. Funct. Mater. (2025) e13167.
[15] Z.-M. Li, W.-Q. Gong, J.-F. Li, S.-X. Zhu, D.-J. Tao, Y. Zhou, Efficient and selective absorption of SO_2 by low-viscosity matrine-based deep eutectic solvents, J. Mol. Liq. 367 (2022) 120521.
[16] G. Cui, N. Zhao, Y. Li, H. Wang, Y. Zhao, Z. Li, J. Wang, Limited number of active sites strategy for improving SO_2 capture by ionic liquids with fluorinated acetylacetonate anion, ACS Sustainable Chem. Eng. 5 (2017) 7985–7992.
[17] K. Zhang, S. Ren, Y. Hou, W. Wu, Efficient absorption of SO_2 with low-partial pressures by environmentally benign functional deep eutectic solvents, J. Hazard. Mater. 324 (2017) 457–463.
[18] F.M. Gaciño, T. Regueira, L. Lugo, M.J.P. Comuñas, J. Fernández, Influence of molecular structure on densities and viscosities of several ionic liquids, J. Chem. Eng. Data 56 (2011) 4984–4999.
[19] D. Song, J. Chen, Density and viscosity data for mixtures of ionic liquids with a common anion, J. Chem. Eng. Data 59 (2014) 257–262.
[20] F. Chu, L. Yang, X. Du, Y. Yang, Mass transfer and energy consumption for CO_2 absorption by ammonia solution in bubble column, Appl. Energy 190 (2017) 1068–1080.
[21] S. Xu, W. Zhao, M. Chai, T. Si, Y. Chen, Q. Jia, Development of SO_2 phase change absorption: viscosity change and component distribution rules, Energy Fuel. 33 (2019) 10029–10038.
[22] S. Zeng, X. Zhang, L. Bai, X. Zhang, H. Wang, J. Wang, D. Bao, M. Li, X. Liu, S. Zhang, Ionic-liquid-based CO_2 capture systems: structure, interaction and process, Chem. Rev. 117 (2017) 9625–9673.
[23] A. Tagawa, N. Dohi, Y. Kawase, Volumetric gas-liquid mass transfer coefficient in aerated stirred tank reactors with dense floating solid particles, Ind. Eng. Chem. Res. 51 (2012) 1938–1948.
[24] R. Petříček, T. Moucha, J.F. Rejl, L. Valenz, J. Haidl, T. Čmelíková, Gas-liquid-solid volumetric mass transfer coefficient and impeller power consumptions for industrial vessel design, Int. J. Heat Mass Tran. 121 (2018) 653–662.
[25] X. Zhang, D. Bao, Y. Huang, H. Dong, X. Zhang, S. Zhang, Gas-liquid mass-transfer properties in CO_2 absorption system with ionic liquids, AIChE J. 60 (2014) 2929–2939.
[26] Y. Chen, Z. Yang, X. Lu, X. Ji, Mass-transfer kinetics of CO_2 in a hybrid choline-2-pyrrolidine-carboxylic acid/polyethylene glycol/water absorbent, J. Mol. Liq. 336 (2021) 116383.
[27] G. Zarca, I. Ortiz, A. Urtiaga, Recovery of carbon monoxide from flue gases by reactive absorption in ionic liquid imidazolium chlorocuprate(I): mass transfer coefficients, Chin. J. Chem. Eng. 23 (2015) 769–774.
[28] M. Martín, F.J. Montes, M.A. Galán, Mass transfer rates from bubbles in stirred tanks operating with viscous fluids, Chem. Eng. Sci. 65 (2010) 3814–3824.
[29] G.A. Whyatt, C.J. Freeman, A. Zwoster, D.J. Heldebrant, Measuring nitrous oxide mass transfer into non-aqueous CO_2BOL CO_2 capture solvents, Ind. Eng. Chem. Res. 55 (2016) 4720–4725.
[30] W.G. Whitman, The two film theory of gas absorption, Int. J. Heat Mass Tran. 5 (1962) 429–433.
[31] C. Wang, Z. Xu, C. Lai, X. Sun, Beyond the standard two-film theory: computational fluid dynamics simulations for carbon dioxide capture in a wetted wall column, Chem. Eng. Sci. 184 (2018) 103–110.
[32] J. Tan, Y.C. Lu, J.H. Xu, G.S. Luo, Mass transfer characteristic in the formation stage of gas-liquid segmented flow in microchannel, Chem. Eng. J. 185–186 (2012) 314–320.
[33] J. Zhang, T. Lu, Efficient evaluation of electrostatic potential with computerized optimized code, Phys. Chem. Chem. Phys. 23 (2021) 20323–20328.
[34] T. Lu, F. Chen, Multiwfn: a multifunctional wavefunction analyzer, J. Comput. Chem. 33 (2012) 580–592.
[35] M. Guin, G.N. Patwari, S. Karthikeyan, K.S. Kim, Do N-heterocyclic aromatic rings prefer π-stacking? Phys. Chem. Chem. Phys. 13 (2011) 5514–5525.
[36] P. Liu, K. Cai, X. Zhang, X. Wang, M. Xu, F. Liu, T. Zhao, Rich ether-based protic ionic liquids with low viscosity for selective absorption of SO_2 through multisite interaction, Ind. Eng. Chem. Res. 61 (2022) 5971–5983.
[37] M.J. Monteiro, R.A. Ando, L.J.A. Siqueira, F.F. Camilo, P.S. Santos, M.C.C. Ribeiro, R.M. Torresi, Effect of SO_2 on the transport properties of an imidazolium ionic liquid and its lithium solution, J. Phys. Chem. B 115 (2011) 9662–9670.
[38] F. Zhao, M. Song, Q. Liu, Y. Cheng, H. Kang, S. Liu, Z. Lei, Thermodynamic and molecular mechanisms of ionic liquids for acetylene dehydration, AIChE J. 70 (2024) e18412.
[39] W. Wu, J. Zhang, Y. Ma, H. Zhang, Z. Cai, Y. Cao, K. Huang, L. Jiang, Ionic liquid-based hybrid acidic catalysts enabling phase splitting and reactive separation for methyl esterification of long-chain fatty acids, Chem. Eng. Sci. 311 (2025) 121595.
[40] M. Jin, Y. Hou, W. Wu, S. Ren, S. Tian, L. Xiao, Z. Lei, Solubilities and thermodynamic properties of SO_2 in ionic liquids, J. Phys. Chem. B 115 (2011) 6585–6591.
[41] E. Dumont, H. Delmas, Mass transfer enhancement of gas absorption in oil-in-water systems: a review, Chem. Eng. Process 42 (2003) 419–438.

[42] C. Xu, Z. Qian, J. Wang, C. Che, B. Sun, Modeling selective absorption of H_2S from a gas mixture containing CO_2 within rotating packed bed based on surface renewal theory, Chem. Eng. Sci. 302 (2025) 120813.
[43] D. Yang, M. Hou, H. Ning, J. Ma, X. Kang, J. Zhang, B. Han, Reversible capture of SO_2 through functionalized ionic liquids, ChemSusChem 6 (2013) 1191–1195.
[44] D. Deng, Y. Jiang, X. Liu, Investigation of furoate-based ionic liquid as efficient SO_2 absorbent, New J. Chem. 41 (2017) 2090–2097.
[45] G. Cui, S. Lyu, H. Wang, Z. Li, R. Zhang, J. Wang, Tuning the structure of pyridinolate-based functional ionic liquids for highly efficient SO_2 absorption, Fuel 303 (2021) 121311.
[46] L. Jiang, M. Pan, S. Wang, Z. Zhao, H. Tao, W. Lin, H. Li, G. Shi, C. Wang, Tunable and facile preparation of chelate-based ionic liquids for highly efficient SO_2 separation under low concentration in flue gas, Sep. Purif. Technol. 318 (2023) 123979.
[47] K. Zhang, S. Ren, X. Yang, Y. Hou, W. Wu, Y. Bao, Efficient absorption of low-concentration SO_2 in simulated flue gas by functional deep eutectic solvents based on imidazole and its derivatives, Chem. Eng. J. 327 (2017) 128–134.